Introduction of an Electromagnetism Module in LS-DYNA for Coupled Mechanical-Thermal-Electromagnetic Simulations

Pierre L'Eplattenier[1)], Grant Cook[1)], Cleve Ashcraft[1)], Mike Burger[1)], Jose Imbert[2)] and Michael Worswick[2)]

[1)] Livermore Software Technology Corporation, 7374 Las Positas Road, Livermore, CA 94551, USA, Pierre@lstc.com
[2)] Department of Mechanical and Mechatronics Engineering, University of Waterloo, Waterloo, Ontario, Canada

A new electromagnetism module is being developed in LS-DYNA for coupled mechanical/thermal/electromagnetic simulations. One of the main applications of this module is Electromagnetic Metal Forming. The electromagnetic fields are solved using a Finite Element Method for the conductors coupled with a Boundary Element Method for the surrounding air/insulators. Both methods use elements based on discrete differential forms for improved accuracy. The physics, numerical methods and capabilities of this new module are presented in detail as well as its coupling with the mechanical and thermal solvers of LS-DYNA. This module is then illustrated on two Electromagnetic Metal Forming cases, the forming of an aluminum sheet on a conical die using a spiral coil, and the forming of an aluminum sheet on a v-shaped die using a "double pancake" coil. The experimental setups are presented as well as comparisons between experimental and numerical results.

Keywords: Modelling, Finite Element Method (FEM), Boundary Element Method (BEM), Electromagnetic Metal Forming (EMF).

DOI: 10.2374/SRI08SP152; submitted on 19 Septemeber 2008, accepted on 12 January 2009

Introduction

LS-DYNA is a highly advanced general-purpose nonlinear finite element program that is capable of simulating complex real world problems. It is suitable to investigate phenomena that involve large deformations, sophisticated material models and complex contact conditions [1]. LS-DYNA allows running an analysis explicitly or implicitly and combining different disciplines such as coupled thermal analysis, fluid dynamics, fluid-structure interaction, SPH (smooth Particle Hydro-dynamics), EFG (Element Free Galerkin). Metal forming is one of LS-DYNA's main applications, with capabilities that allow one to simulate rolling, extrusion, forging, casting, spinning, ironing, super-plastic forming, sheet metal stamping, profile rolling, deep drawing, hydro-forming, multi-stage processing, springback, hemming.

An electromagnetism (EM) module is under development in LS-DYNA in order to perform coupled mechanical/thermal/electromagnetic simulations [2]. This module allows us to introduce some source electrical currents into solid conductors, and to compute the associated magnetic field, electric field, as well as induced currents. These fields are computed by solving the Maxwell equations in the eddy-current approximation. The Maxwell equations are solved using a Finite Element Method (FEM) [3] for the solid conductors coupled with a Boundary Element Method (BEM) [4] for the surrounding air (or insulators). Both the FEM and the BEM are based on discrete differential forms (Nedelec-like elements [5]).

Electromagnetic Metal Forming (EMF) is one of the main applications of this development. EMF is a high velocity forming process where the force deforming the workpiece is a magnetic one, generated by an electrical current induced in the workpiece by a coil. Much work has shown that the formability can be significantly increased, wrinkling can be mitigated, springback can be reduced and so forth. Forming of aluminum has been the main focus of EMF, due to its potential as a means of reducing automobile weight.

Other processes could also be simulated, where magnetic pressure induces mechanical stress and deformations and/or the Joule effect induces a heating process: magnetic metal cutting, magnetic metal welding, very high magnetic pressure generation, rail-gun type apparatus, computation of the stresses and deformations in various coils, magnetic flux compression, induced heating and so forth.

In the first part, the EM module will be presented, the FEM part, the BEM part, and the coupling with external circuits. In a second part, the coupling of the EM module with the rest of LS-DYNA, and in particular with the mechanical and thermal modules will be presented. In the third part, some comparisons between experimental and numerical results are presented on two EMF cases: the forming of an aluminum sheet on a conical die using a spiral coil, and the forming of an aluminum sheet on a v-shaped die using a "double pancake" coil.

Presentation of the Electromagnetism Module

Scalar potential and Modified vector potential formulation. Let Ω be a set of multiply connected conducting regions. The surrounding insulator exterior regions will be called Ω_e. The boundary between Ω and Ω_e is called Γ, and the (artificial) boundary on Ω at the end of the meshing region (hence where the conductors are

connected to an external circuit) is called Γ_c. In the following, we will denote $\vec{n}$ as the outward normal to surfaces Γ or Γ_c. The electrical conductivity, permeability and permittivity are called σ, μ and ε respectively. In Ω_e, we have $\sigma = 0$ and $\mu = \mu_0$.

We start with the Maxwell equations in the so called low frequency or "eddy-current" approximation, which is valid for good enough conductors with low frequency varying fields such that the condition $\varepsilon \frac{\partial \vec{E}}{\partial t} \prec\prec \sigma \vec{E}$ is satisfied, where $\vec{E}$ is the electric field. This approximation implies a divergence free current density and no free charge accumulation. It is very well satisfied in EMF experiments.

$$\vec{\nabla} \times \vec{E} = -\frac{\partial \vec{B}}{\partial t} \tag{1}$$

$$\vec{\nabla} \times \frac{\vec{B}}{\mu} = \vec{j} \tag{2}$$

$$\nabla \bullet \vec{B} = 0 \tag{3}$$

$$\nabla \bullet \varepsilon \vec{E} = 0 \tag{4}$$

$$\nabla \bullet \vec{j} = 0 \tag{5}$$

$$\vec{j} = \sigma \vec{E} + \vec{j}_S \tag{6}$$

where $\vec{B}$ is the magnetic flux density, $\vec{j}$ the total current density, and $\vec{j}_S$ is a divergence free source current density.

The divergence condition (3) allows writing $\vec{B}$ as

$$\vec{B} = \vec{\nabla} \times \vec{A} \tag{7}$$

where we introduce the magnetic vector potential $\vec{A}$ [6]. Equation (1) then implies that the electric field is given by

$$\vec{E} = -\vec{\nabla}\phi - \frac{\partial \vec{A}}{\partial t} \tag{8}$$

where ϕ is the electric scalar potential. We use the Gauge condition

$$\nabla \bullet \sigma \vec{A} = 0 \tag{9}$$

which allows a separation of the vector potential from the scalar potential in the equations. Equations (5), (6), (8) and (9) imply:

$$\nabla \bullet \sigma \vec{\nabla} \phi = 0 \tag{10}$$

And equations (2), (7), (6) and (8) imply:

$$\sigma \frac{\partial \vec{A}}{\partial t} + \vec{\nabla} \times \frac{1}{\mu} \vec{\nabla} \times \vec{A} + \sigma \vec{\nabla} \phi = \vec{j}_S \tag{11}$$

Equations (10) and (11) represent the Maxwell equations in term of the 2 potentials. They come with the following boundary conditions:

$$\vec{n} \bullet \vec{\nabla} \phi = 0 \text{ on } \Gamma \tag{12}$$

$$\phi = \phi_c \text{ on } \Gamma_c \tag{13}$$

and

$$\vec{n} \times \vec{\nabla} \times \vec{A} = \vec{A}_e \text{ on } \Gamma \tag{14}$$

$$\vec{n} \times \vec{A} = A_c \text{ on } \Gamma_c \tag{15}$$

Equation (13) allows the connection of the conductors to a voltage source and equation (15) to a current source, although we will show in the following that the connection with a current source can also be done through the BEM part of the system, allowing more flexibility when using conductors with non trivial topologies.

Once the potentials are computed, the electromagnetic fields are given by Equations (8), (7) and (6).

Finite element method. Equations (10) and (11) are solved in the conductors with a Finite Element Method using a library called "FEMSTER" developed at the Lawrence Livermore National Laboratories [7]. FEMSTER provides discrete numerical implementations of the concepts from differential forms (often referred as Nedelec elements) [8-9]. These include in particular the exterior derivatives of gradient, curl and divergence, and also the div-grad, curl-curl and grad-div operators. FEMSTER provides four forms of basis functions, called 0-forms, 1-forms, 2-forms and 3-forms, defined on hexahedra, tetrahedra and prisms. At this time, only hexahedral elements are available in the EM module of LS-DYNA. The two other types will soon be available.

0-forms are continuous scalar basis functions that have a well defined gradient, the gradient of a 0-form being a 1-form. At first order, the degrees of freedom associated with a 0-form are the values of the scalar field at the nodes of the mesh. In our particular case, the 0-forms are used for the discretization of the scalar potential ϕ.

1-forms are vector basis functions with continuous tangential components but discontinuous normal components. They have a well defined curl, the curl of a 1-form being a 2-form. At first order, the degrees of freedom of a 1-form are its line integrals along the edges of the mesh. They are used for the discretization of the electric field $\vec{E}$, the magnetic field $\vec{H}$ and the vector potential $\vec{A}$.

2-forms are vector basis functions with continuous normal components across elements but discontinous tangential components. They have a well defined divergence, the divergence of a 2-form being a 3-form. At first order, the degrees of freedom of a 2-form are its fluxes across all the facets of the mesh. They are used for the discretization of the magnetic flux density $\vec{B}$, and the current density $\vec{j}$.

Finally, the 3-forms are discontinuous scalar basis functions which cannot be differentiated. Their degrees of freedom at first order are their integrals over the elements of the mesh.

These basis functions define spaces with an exact representation in the De-Rham sequence [7]. They also exactly satisfy numerical relations such as curl(grad)=0 or div(curl)=0, which are very important for conservation laws when solving the systems [10]. At first order, they allow one to solve partial differential equation at an integrated "Stokes theorem" level which proves to be very efficient and accurate, even on low density meshes, compared to using vector basis functions [10].

We will denote W^0, $\vec{W}^1$, $\vec{W}^2$, and W^3 as the basis functions associated respectively with the 0, 1, 2, and 3-forms. Equation (10) is projected against 0-forms basis functions and Equation (11) against 1-forms to give, after using the appropriate Greens vector identities and the boundary conditions (12) - (15) [10].

$$\int_{\Omega} \sigma \vec{\nabla}\phi \bullet \vec{\nabla} W^0 d\Omega = 0 \tag{16}$$

$$\int_{\Omega} \sigma \frac{\partial \vec{A}}{\partial t} \bullet \vec{W}^1 d\Omega + \int_{\Omega} \frac{1}{\mu} \vec{\nabla}\times\vec{A} \bullet \vec{\nabla}\times\vec{W}^1 d\Omega = - \int_{\Omega} \sigma \vec{\nabla}\phi \bullet \vec{W}^1 d\Omega + \frac{1}{\mu}\int_{\Gamma} [\vec{n}\times(\vec{\nabla}\times\vec{A})] \bullet \vec{W}^1 d\Gamma \tag{17}$$

or equivalently after decomposing $\vec{A}$ and ϕ respectively on the 0-form and 1-form basis functions:

$$S^0(\sigma)\varphi = 0 \tag{18}$$

$$M^1(\sigma)\frac{da}{dt} + S^1(\frac{1}{\mu})a = -D^{01}(\sigma)\varphi + Sa \tag{19}$$

where we introduce the 0-form stiffness matrix S^0, the 1-form mass matrix M^1, the 1-form stiffness matrix S^1 and the 0-1 form derivative matrix D^{01} [10]. The last term of Equation (19) which involves the "outside matrix stiffness" S is computed using a Boundary Element Method.

Boundary Element Method. In order to compute Sa, an intermediate variable "surface current" $\vec{k}$ is introduced. This surface current, defined on the boundary Γ is such that it produces the same vector potential (and thus $\vec{B}$ field) in the exterior regions Ω_e as the actual volume current flowing through the conductors [11]:

$$\vec{A}(x) = \frac{\mu_0}{4\pi}\int_{\Gamma} \frac{1}{|x-y|}\vec{k}(y)dy \tag{20}$$

for all $x \in \Omega_e$ (and in particular for all $x \in \Gamma$).

One then has:

$$[\vec{n}\times(\vec{\nabla}\times\vec{A})](x) = \frac{\mu_0}{2}\vec{k}(x) - \frac{\mu_0}{4\pi}\int_{\Gamma}\frac{1}{|x-y|^3}\vec{n}\times[(\vec{x}-\vec{y})\times\vec{k}(y)]dy \quad \text{for } x \to x_0 \in \Gamma \tag{21}$$

When projecting these equations on the 1-forms basis functions for $\vec{A}$ and the "twisted" 1-forms $\vec{V}^1(x) = \vec{n}\times\vec{W}^1(x)$ for $\vec{k}$ one gets the following matrix equations:

$$Pk = Da \tag{22}$$

$$Sa = Qk \equiv Q_S k + Q_D k \tag{23}$$

where we introduce the BEM matrices

$$P_{i,j} = \frac{\mu_0}{4\pi}\iint_{\Gamma_x\Gamma_y}\frac{1}{|x-y|}\vec{V}_i^1(x)\bullet\vec{V}_j^1(y)d\Gamma_x d\Gamma_y,$$

$$D_{i,j} = \int_{\Gamma_x}\vec{V}_i^1(x)\bullet\vec{W}_j^1(x)d\Gamma_x \tag{24}$$

$$Q_{S\,i,j} = \frac{1}{2}\int_{\Gamma_x}\vec{W}_i^1(x)\bullet\vec{V}_j^1(x)d\Gamma_x, \tag{25a}$$

$$Q_{D_{i,j}} = -\frac{1}{4\pi}\iint_{\Gamma_x\Gamma_y}\frac{1}{|x-y|^3}\vec{W}_i^1(x)\bullet\{\vec{n}_x\times[(\vec{x}-\vec{y})\times\vec{V}_j^1(y)]\}d\Gamma_x d\Gamma_y \tag{25b}$$

The BEM method is very appealing since it does not need a mesh in the air surrounding the conductors. It thus avoids the meshing problems associated with the air, which can be significant for complicated conductor geometries. Also, for very small gaps between conductors, an air mesh could include a large number of very small and distorted elements. Even more importantly, the BEM avoids remeshing problems which arise when using an air mesh around moving conductors. Another advantage of the BEM is that it does not need the introduction of somewhat artificial infinite boundary conditions.

The main disadvantage of the BEM is that it generates fully dense matrices like P and Q_D (24,25) in place of the sparse FEM matrices. This causes a-priori high memory requirements as well as longer CPU time to assemble the matrices and solve the linear systems. In order to limit the memory requirement, a domain decomposition is done on the BEM mesh, which splits the BEM matrices into sub-blocks. On the non-diagonal sub-blocks, a low rank approximation based on a rank revealing QR decomposition is performed. For sub-blocks corresponding to far away domains, the rank can be significantly smaller than the size of the sub-block, thus reducing the storage of the sub-block. We typically see reductions of by factors around 20 between the fully dense matrix and the block matrix with low rank approximations. This low rank approximation also speeds up the matrix * vector operation used intensively in the iterative method to solve the BEM system (22). This method still needs the

assembly of the full sub-blocks before doing the low rank approximation, generating a time consuming assembly process. We currently are working on methods for directly generating the low rank approximations of the sub-blocks.

The matrices P and Q_D (24-25b) become singular or nearly singular as $x \to y$, i.e. for self face integrals or integrals over neighbor faces with a common edge or a common node. Special methods have been included such as the ones described in [12] and [13]. These methods also allow more accurate integration on inhomogeneous faces, i.e. faces with large aspect ratio.

Divergence free surface current, connection with external circuits. The surface current $\vec{k}$ is an equivalent boundary current to the actual volume current through the volume of the conductor and needs to be divergence free [11]. However, the twisted 1-forms basis functions $\vec{V}^1$ do not satisfy this divergence free constraint. We first added it as an external constraint to the BEM system (22). More recently, we introduced the so called "loop-star" solenoidal-irrotational decomposition into the divergence free "loop" basis functions and the other ones [14-15]. At first order, a twisted 1-form associated with a surface edge represents a surface current flowing across the edge, i.e. with a unit surface flux across the edge and a zero surface flux across all the other surface edges. A loop basis function associated with a node can be seen as a linear combination with coefficients +1 or -1 of 1-forms associated with all the edges originating from the node, so that it represents a (divergence-free) current flowing around the node. One can show that when using first order basis functions, the loop basis function associated with all the nodes of the surface mesh (except one) form a complete basis of the divergence free currents for topologically simple conductors [14]. For non-simple conductors, i.e. containing holes or "handles", a few extra non-local basis functions that we call "global currents" need to be added. For example in the case of a torus, two extra global currents need to be added, one corresponding to a current flowing in the toroidal direction, and one corresponding to a current flowing in the poloidal direction.

An algorithm based on the construction of a spanning tree on the surface mesh has been developed to automatically count the number of connected parts, get their topologies by computing the "Betti numbers" [16], and in particular the number of global currents and then set the global current basis functions as linear combinations of the 1-form basis functions. The degrees of freedom associated with the global currents are used to impose current vs time constraints as a simple dirichlet constraint in the BEM system (one dirichlet constraint per imposed current). This method allows imposing currents in geometries where more traditional methods using dirichlet conditions on the FEM system (15) would require the introduction of cuts and/or multi-valued degrees of freedom. The above mentioned toroidal current in a torus is such an example. The use of loop and global current basis functions also gives an easy way to compute the self and mutual inductances, by solving BEM systems (22) with simple dirichlet constraints. In this manner, the conductors can be connected to a current source, a voltage source, or an R,L,C circuit.

Global integration scheme. The time integration of the FEM system (19) is done using an implicit backward euler method [10]:

$$[M^1(\sigma) + dtS^1(\frac{1}{\mu})]a^{t+1} = M^1(\sigma)a^t - dtD^{01}(\sigma)\varphi^{t+1} + dtSa^{t+1} \tag{26}$$

The BEM part of the right hand side $dtSa^{t+1}$ also is implicit which proved to substantially improve the stability, thus allowing larger time steps. It is computed by solving the BEM system (22)(23) coupled with the FEM system (19) in an iterative way:

$$Pk_{n+1}^{t+1} = Da_n^{t+1} \tag{27}$$

$$[M^1(\sigma) + dtS^1(\frac{1}{\mu})]a_{n+1}^{t+1} = M^1(\sigma)a^t - dtD^{01}(\sigma)\varphi^{t+1} + dtQk_{n+1}^{t+1} \tag{28}$$

until convergence on both k_n^{t+1} and a_n^{t+1}.

The FEM System (28) is solved using a direct solver. The BEM system (27) is solved using a pre-conditioned gradient method. The diagonal of the matrix has been used as a pre-conditioner. More recently, the diagonal block has been used instead [17], with significant reduction in the number of required iterations (typically by a factor between 1.5 and 3).

Coupling of the EM Module with LS-DYNA

Mechanical solver. Once the EM fields have been computed, the Lorentz force $\vec{F} = \vec{j} \times \vec{B}$ is evaluated at the nodes and added to the mechanical solver. The mechanical and electromagnetic solvers each have their own time step. For a typical EMF simulation, the mechanical time step is about 10 times smaller than the electromagnetic one. At this time, the explicit mechanical solver of LS-DYNA is used when coupled with electromagnetism. The mechanical module computes the deformation of the conductors and the new geometry is used to compute the EM fields in a Lagrangian way.

Since the EM module is fully integrated in LS-DYNA, all the material models are available. LS-DYNA provides more than 130 metallic and non-metallic material models, many of them equipped with failure criteria, such as metals, plastics, visco-elastic, elasto-viscoplastic, glass, foam, elastomers and rubbers. Included also are strain rate and temperature dependant plasticity models such as Johnson-Cook [18], Zerilli-Armstrong [19] or Steinberg [20] models, which are particularly suitable for high speed forming simulations. Numerous equations of state are also available. These models can be used on an extensive

element library with both under-integrated and fully-integrated element formulations. It includes different solid elements, thick shells, different 3- and 4-node shells and beams. At this time, the EM module is only available on solid elements. It should soon be extended to shells with appropriate treatment of the diffusion of the EM fields.

Finally, efficient contact algorithms have been developed for the mechanical solver, and over 25 different contact options are available. At this time, the contact purely is mechanical and thermal, not electromagnetic, i.e. a current cannot flow from one conductor to another if they come in contact during the simulation. This will be added as well as an electromagnetic sliding contact capability, necessary for rail-gun applications.

Thermal solver. The Joule heating term $j^2/\sigma\rho$ is added to the thermal solver allowing to update the temperature. Several thermal models are available, isotropic, orthotropic, isotropic with phase change and so forth. The temperature can be used in turn in an electromagnetic equation of state to update the electromagnetic parameters, mainly the conductivity σ. At this time, a Burgess model [21] has been introduced**.**

Input-output. Electromagnetic cards have been added to the standard LS-DYNA card list used to create the input deck. The LS-PREPOST software can be used to visualize the electromagnetic fields - current density, electric field, magnetic flux density, Lorentz force, joule heating, conductivity, surface current - in the same environment as the mechanical and thermal fields. These include fringe component, iso-contour, vector plots at a given time, and also time histories on chosen elements.

Comparisons between Experimental and Numerical Results on EMF cases

We now present some comparisons between experimental and numerical results on actual metal forming experiments. Dealing with real life models allows us to show the code's capability to handle complicated structures. More quantitative comparisons on simpler cases have already been presented in [2].

Case 1: forming of conical samples with a spiral coil

Experimental setup. The first case deals with the electromagnetic forming of a 1mm thick aluminum sheet on a conical die. This forming represents part of the work performed by some of the authors at the Department of Mechanical Engineering, University of Waterloo, Ontario, Canada. It is described in [22-24] where details of the experimental procedures can be found. Conical samples of 40° side angle were analysed for this study. A seven-turn brass spiral coil with a nominal diameter of 100 mm and a maximum diameter of 115 mm at the end was used. An IAP Magnepress magnetic pulse generator with a storage capacity of 22.5 kJ at 15kV was used to form the samples. The currents used to form these samples were unfortunately not measured. The charge voltage was the recorded input parameter and for the samples in question it was 8000 V.

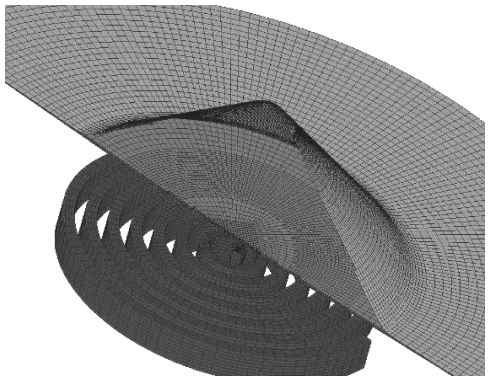

Figure 1. Mesh of case 1. Only half of the sheet and die are represented.

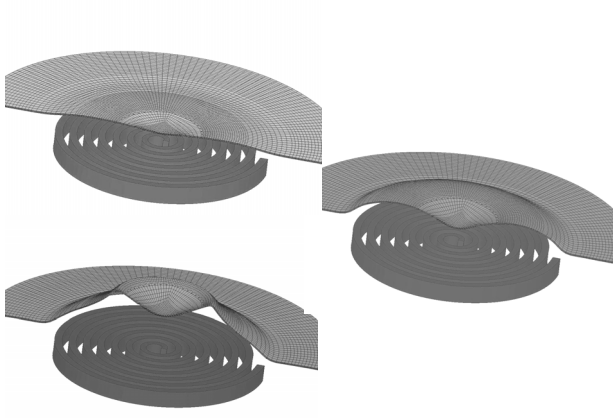

Figure 2. 3D shape of the sheet for case 1 (only half of the sheet is represented), at 45μs (top left), 70μs (middle right) and 100μs (bottom left).

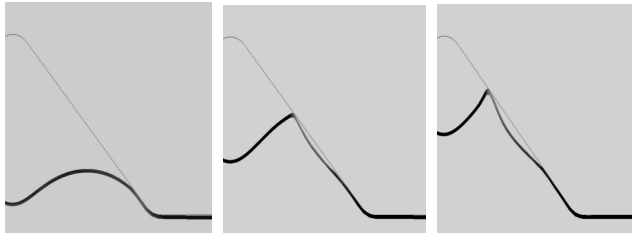

Figure 3. Case 1: detail of the rebounding of the sheet from the die: cross section of the sheet (thick line) and die (thin line) at 70μs (left), 100μs (middle) and 130μs (right).

Numerical simulation. A hexahedral 3D mesh was built for the coil and the workpiece, and shell elements were used for the die. The mesh is composed of 20736 elements for the coil, 32320 for the aluminium sheet, with 4 elements through the thickness, and 17220 shells for the die. This mesh generated 23056 BEM faces, and 23163 BEM nodes (and hence 23163 degrees of freedom in the BEM system). **Figure 1** shows the mesh at initial time.

Comparison between experiment and simulation. **Figure 2** shows the evolution of the shape of the plate. **Figure 3**

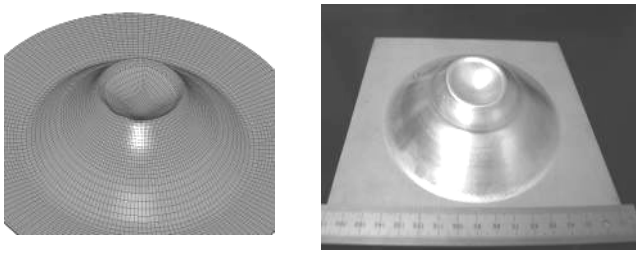

Figure 4. Case 1: numerical (left) and experimental (right) final shape of the sheet.

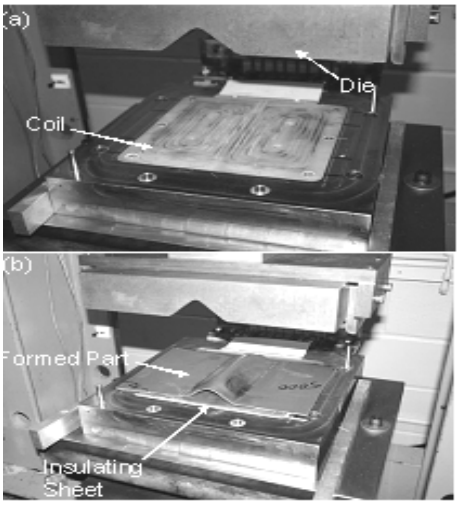

Figure 5. Case 2: Experimental apparatus for the v-channel samples.

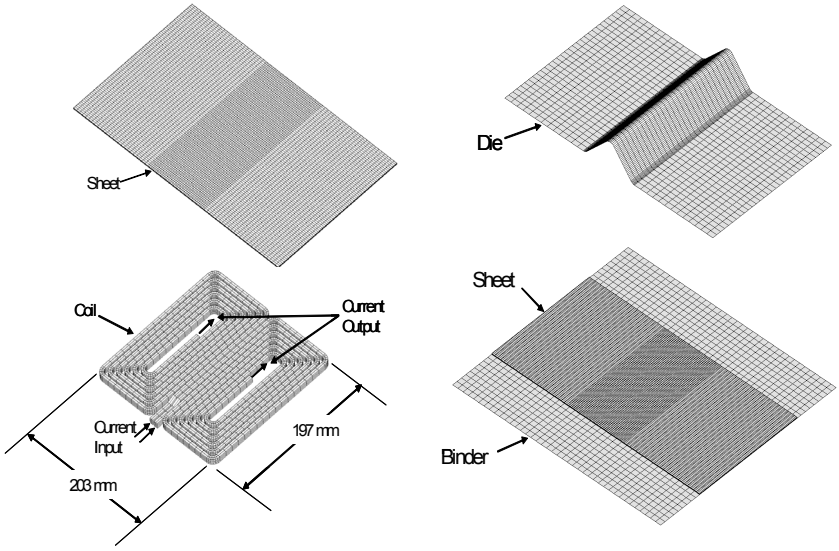

Figure 6. Case 2: Mesh used for the v-channel model. The binder and die were not included in the EM calculation.

shows details of the rebounding of the sheet from the die. **Figure 4** shows a comparison between the numerical and experimental final shape of the sheet. The final shape shows a good agreement. One can notice that the shape does not match the shape of the die, due to rebounding of the plate from the die and a non-uniform magnetic pressure on the sheet, with a significantly lower pressure at the centre. This low pressure area is reflected in the current density plots, and is due to the shape of the coil.

Case 2: forming of V-shaped samples with a "double pancake" coil

Experimental setup. For these experiments, also performed at the University of Waterloo, a flat "double pancake" coil encased in Garolite and epoxy was used. The coil was designed to get a close to uniform magnetic pressure on a large area, in contrast to the spiral coil. The coil was connected to a Pulsar MPW 20 – Research Edition magnetic pulse generator, which consists of a capacitor bank and a power supply to deliver the current to the capacitors at the required specifications. The pulse generator has a nominal maximum energy capacity of 20 kJ and charging voltage of 9 kV. A triangular or "v" shaped die with a side angle of 40° was chosen, since it was the maximum safe angle reached with the conical samples studied in [22]. The material used was AA 5754 in 1 mm sheets in samples of 197 x 305 mm. The metal samples were placed over the coil with sheets of an insulating material (Kapton©) separating the coil from the sample for additional insulation. The sheet was then clamped using a hydraulic press. Two sets of samples were formed, one where the samples did not make impact with the die and the other where the material impacted the die. These samples were formed using 3000 V and 5000 V respectively. **Figure 5** shows the apparatus used for these experiments.

Numerical simulation. The coils and workpieces were modeled using eight node hexagonal solid elements. The sheet was modeled with an elastic-plastic piecewise linear plasticity model described in [22,23]. An isotropic quasi-static model was deemed acceptable since AA 5754 has shown little strain rate sensitivity [25]; however, the material has not been tested under the conditions encountered during EMF. The coils were modeled as elastic materials with a Young's Modulus of 97 GPa. Both experimental and numerical results showed no noticeable deformation of the coil. The binders and dies were modeled as rigid bodies using shell elements, and were

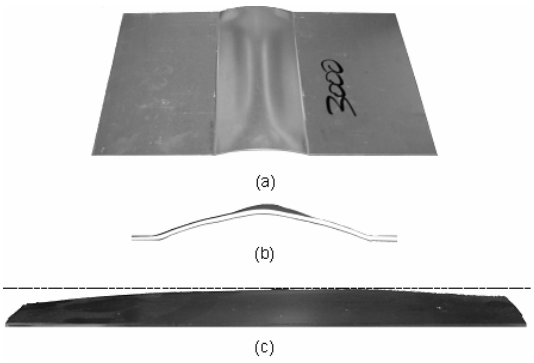

Figure 7. Case 2: v-channel sample formed with a 3000 V charging voltage. The sample did not make contact with the die.

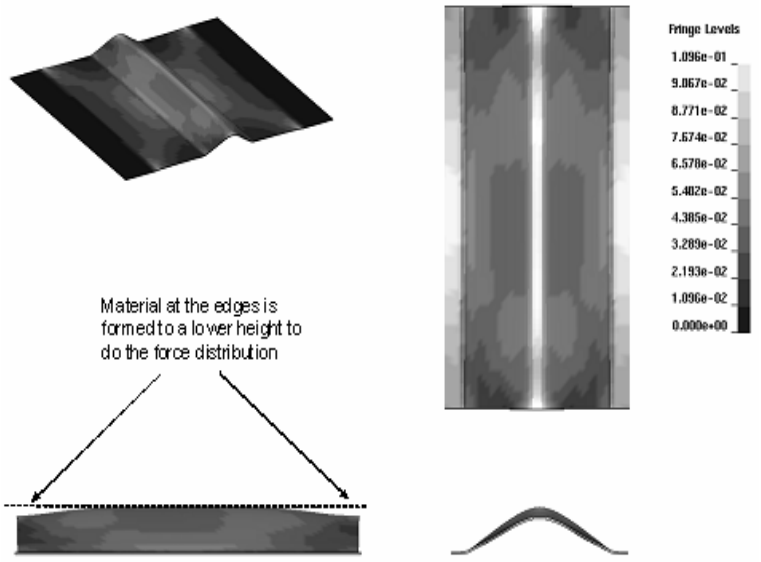

Figure 8. Case 2: numerical final shape for a v-channel forming process with a 3000 V charging voltage. Contours are of effective plastic strain, from 0 (black) to 0.11 (white).

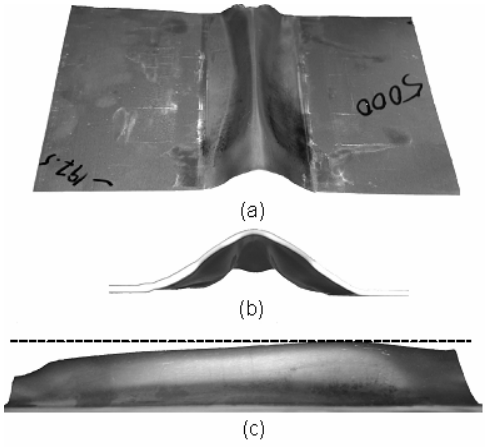

Figure 9. Case 2: v-channel sample formed with a 5000 V charging voltage. The shaded areas indicate where the sample made contact with the die. The uneven forming is attributed to coil imperfections which result in an uneven force distribution.

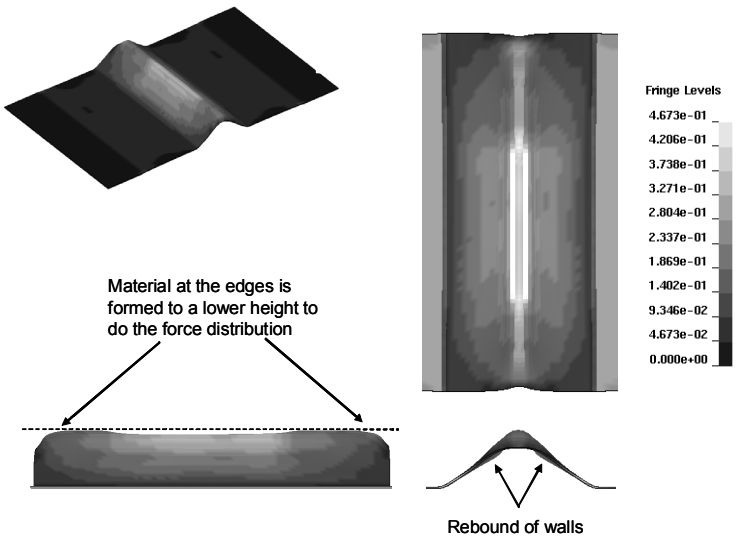

Figure 10. Case 2: numerical final shape for a v-channel forming process with a 5000 V charging voltage. Contours are of effective plastic strain, from 0 (black) to 0.46 (white).

ignored for the electromagnetic calculation. The mesh used for the open channel models is shown in **Figure 6**. The sheet mesh for the open channel simulations had 28 800 elements.

The model was connected to an RLC circuit with the resistance, inductance and capacitance of the system being provided as inputs and the software calculated the current. The values used for the v-channel simulations were; R= 5.96 x10^{-3} Ohms, L= 48.0 x 10^{-6} mH and C= 2.7 x10^{-7} F. A constant conductivity of 25 x 10^{6} $Ohm^{-1}m^{-1}$ was used for the coil and sheet. This simplification results in some inaccuracies; however, for the purposes of this study it was considered acceptable.

Comparison between experiment and simulation. A v-channel sample formed using 3000 V charging voltage where no impact with the die occurred is shown in **Figure 7.** The parts are not formed uniformly, which is an indication that the force distribution is uneven. **Figure 8** shows the numerical final shape for the same case and it can be seen that the major features of the part are predicted. However, the asymmetric height distribution of the samples (Figure 7-c) is not captured by the models.

The samples formed using a charge voltage of 5000 V made contact with the die which resulted in a distinctive shape, as shown in **Figure 9**. The darker areas on the parts are the places where the sheet made contact with the die.

It is apparent that the final part does not correspond to the shape of the v-channel die. The numerical final shape is shown in **Figure 10**. The final shape is the result of the numerical sheet rebounding from the impact with the die. The model captures the general trends; however, there are discrepancies that are likely due, in part, to the difference between the actual coil and the model of it and to the material model. The coil has geometric imperfections, such as uneven heights, which are not accurately reproduced in the mesh for the numerical model. Also, the quasi-static material model used may not be capturing the actual behavior of the material in the forming conditions in question.

Conclusions

The newly introduced Electromagnetism module of LS-DYNA was presented. The electromagnetic fields are computed by solving the Maxwell equations in the eddy-current approximation, using a Finite Element Method for the conductors coupled with a Boundary Element Method for the surrounding air and insulators. Loop basis functions are used to represent the BEM surface current, allowing to handle the divergence free constraint as well as easy connection with external circuits. A 2-dimensional axisymmetric version of the EM module is also available. Some comparisons between experimental and numerical results were presented. Such comparisons are very important to validate the module, and more will be done in the future.

This module is integrated in the 980 version of LS-DYNA, which should be released in 2009. In the mean time, it is available as a "beta version". The near-term future developments for the EM module include new BEM assembly methods, introduction of tetrahedral and wedge elements, development of an Massively Parallel Processor (MPP) version (the rest of LS-DYNA is currently available in MPP, but the EM module is only serial). The planned longer-term developments include the introduction of sliding contact capabilities for the electromagnetism, remeshing capabilities, extension to other solvers (magnetostatics and so forth).

References

[1] LS-DYNA Theory Manual, LSTC.

[2] P. L'Eplattenier, G. Cook, C. Ashcraft, M. Burger, A. Shapiro, G. Daehn, M. Seith: Introduction of an Electromagnetism Module in LS-DYNA for Coupled Mechanical-Thermal-Electromagnetic Simulations, 9th International LS-DYNA Users conference", Dearborn, Michigan, June 2005.

[3] J. Jin: The Finite Element Method in Electromagnetics", Wiley, 1993.

[4] J. Shen: Computational Electromagnetics Using Boundary Elements, Advances In Modelling Eddy Currents, Topics in Engineering Vol 24, Series Eds: C.A. Brebbia and J.J. Connor, Southampton and Boston: Computational Mechanics Publications, 1995.

[5] J.C. Nedelec: A New Family of Mixed Finite Elements in R3, Num. Math, 50 (1986), 57-81.

[6] O. Biro and K. Preis: On the use of the magnetic vector potential in the finite element analysis of three-dimentional eddy currents", IEEE Transaction on Magnetics, 25(1989), No. 4, 3145-3159.

[7] P. Castillo, R. Rieben and D. White: FEMSTER: An object oriented class library of discrete differential forms. In Proceedings of the 2003 IEEE International Antennas and Propagation Symposium, volume 2, pages 181-184, Columbus, Ohio, June 2003.

[8] Z. Ren and A. Razek: Computation of 3-D electromagnetic field using differential forms based elements and dual formulations, International Journal of Numerical Modeling: Electronic Networks, Devices and Fields, 9 (1996), 81-98.

[9] R. Rieben: A Novel High Order Time Domain Vector Finite Element Method for the Simulation of Electromagnetic Devices, Ph-D Thesis, University of California Davis, 2004.

[10] R. Rieben and D. White: Verification of high-order mixed finite element solution of transient magnetic diffusion problems, IEEE Transaction on Magnetics, 42 (2006), No.1, 25-39.

[11] Z. Ren, A. Razek: New technique for solving three-dimentional multiply connected eddy-current problems, IEE Proceedings, Vol. 137, Pt. A, No 3, May 1990.

[12] W. Wang and N. Atalla: A numerical algorithm for double surface integrals over quadrilaterals with a 1/r singularity, Communications in Numerical Methods in Engineering, 13 (1997), 885-890.

[13] S. Sauter: Cubature techniques for 3-D Galerkin BEM", Boundary Elements: Implementation and Analysis of Advanced Algorithms, W. Hackbusch, G. Wittum eds, NNNFM 54, Vieweg-Verlag, 1996, pp. 29-44.

[14] G. Vecchi: Loop-Star Decomposition of Basis Functions in the Discretization of the EFIE, IEEE Transactions on Antennas and Propagation, Vol. 47, No 2, February 1999.

[15] J.L. Volakis, D.B. Davidson: Iterative-Solver Convergence for Loop-Star and Loop-Tree Decompositions in Method-of-Moments Solutions of the Electric-Field Integral Equation, IEEE Antennas and Propagation, 46 (2004), No.3, 80-85.

[16] A. Bossavit: Computational Electromagnetism, Academic Press (Boston), 1998.

[17] K.E. Chen: On a class of preconditioning methods for dense linear systems from boundary elements, SIAM J. Sci. Comput. 20 (1998), No.2, 684-698.

[18] G.R. Johnson and W.H. Cook: Fracture Characteristics of Three Metals Subjected to Various Strains, Strain Rates, Temperatures and Pressures, Engineering Fracture Mechanics, 21 (1985), No 1, 31-48.

[19] F.J. Zerilli and R.W. Armstrong: Dislocation-mechanics-based constitutive relations for material dynamics calculations, J. Appl. Phys., 61 (1987), No. 5, pp. ????

[20] D.J. Steinberg, S.G.Cochran, M.W.Guinan: A Constitutive Model for Metals Applicable at High-Strain Rate, J. Appl. Phys., 51 (1980), 1498.

[21] T.J. Burgess: Electrical resistivity model of metals, 4th Int. Conf. on Megagauss Magnetic-Field Generation and Related Topics, Santa Fe, NM, USA, 1986.

[22] J. M. Imbert: Increased Formability and the Effects of the Tool/Sheet Interaction in Electromagnetic Forming of Aluminum Alloy Sheet", Masters of Applied Science thesis, University of Waterloo, 2005.

[23] J. M. Imbert, M. J. Worswick, S. L. Winkler, S. Golovashchenko, V. Dmitriev: Analysis of the Increased Formability of Aluminum Alloy Sheet Formed Using Electromagnetic Forming. SAE paper number 2005-01-0082.

[24] J.M. Imbert, S. L. Winkler, M. Worswick, D.A. Oliveira, S. Golovashchenko: The Effect of Tool/Sheet Interaction on Damage Evolution in Electromagnetic Forming of Aluminum Alloy Sheet, ASME-Journal of Engineering Materials and Technology, 127 (2005), No. 1, 145-152.

[25] R. Smerd, S. Winkler, C. Salisbury, M. Worswick, D. Lloyd, M. Finn: High Strain Rate Tensile Testing Of Automotive Aluminum Alloy Sheet, submitted for publication to the International Journal of Impact Engineering, November 2004.